Effects of host-molecule transport polarities on the transient electroluminescence decay and efficiency roll-off of doped organic light-emitting diodes

Jing Chen,[1] Xi Zhao,[1] Bo Wang,[1] Junhong Liu,[1] Xiantong Tang,[2,1,*] Teng Peng,[1] and
Zuhong Xiong [1,†]

[1] *Chongqing Key Laboratory of Micro&Nano Structure Optoelectronics, School of Physical Science and Technology, Southwest University, Chongqing 400715, People's Republic of China*
[2] *School of Science, Chongqing University of Posts and Telecommunications, Chongqing 400065, People's Republic of China*

Dispersing organic fluorophores into a host matrix for doped organic light-emitting diodes (OLEDs) is an efficient method to improve the device optoelectronic performance. However, the effects of host-molecule polarity (i.e., the preference of charge-carrier transporting ability) on the carrier dynamic processes and efficiency roll-off of OLEDs are still vague. Herein, we find that the transient electroluminescence (TEL) decay behaviors reflecting the carrier dynamics depend remarkably on the host-molecule polarity. That is, the TEL curves of devices with the bipolar transport host decay slowly after turning off the voltage pulse, while those from devices with the unipolar one decay rapidly within several microseconds. In addition, through the comprehensive measurements and analyses of TEL, magnetoconductance responses, capacitance curves, and electroluminescence efficiency measured from the control devices with unipolar, bipolar, and mixed unipolar host materials, we conclude that all of these experimental methods, especially the TEL measurement, can serve as effective tools to obtain insights into the complex charge-carrier dynamic processes in devices possessing different charge-balance states. We propose an alternative experimental approach that reducing the emission-layer (EML) thickness appropriately in OLEDs with unipolar hosts can greatly suppress their efficiency roll-off. Specifically, the critical current density of J_0 (i.e., the current density at which the external quantum efficiency drops to half of its maximum value) obtains a significant increase from 37.14 mA/cm^2 to 149.76 mA/cm^2 in the unipolar host-based device by decreasing the EML thickness from 60 to 20 nm. Thus, this work not only presents the key role of host-molecule polarity in charge dynamic processes but also provides a good methodology for visualizing these intricate processes and alleviating the efficiency roll-off of OLEDs.

I. INTRODUCTION

Organic light-emitting diodes (OLEDs) have undergone significant advancements in the application area of solid-state lighting and flat-panel displays since the pioneering research work conducted by Tang and VanSlyke in 1987 [1]. During the development process of OLEDs, extensive efforts have been invested in exploring the fundamental physical microscopic processes of charge carriers for improving device optoelectronic performance [2–5]. Transient electroluminescence (TEL) has always been employed as a highly sensitive measurement technique to detect the physical processes of carrier transport, charge accumulation, and exciton interaction in OLEDs [6–8]. This is because the measured TEL characteristic, especially the TEL decay behaviors after turning off the voltage

*tangxt@cqupt.edu.cn
†zhxiong@swu.edu.cn

pulse, strongly depends on the carrier dynamic processes. However, the factors that can influence the carrier dynamics and the TEL decay behavior are diverse and complex. In 2007, Kondakov reported that the delayed TEL decay in anthracene-derivative-based fluorescent OLEDs originated from the excitonic interaction of the triplet-triplet annihilation (TTA) process [9]. In 2010, Shinar *et al.* demonstrated that the μs-long TEL decay tails from doped OLEDs were generated by the radiative recombination of the trapped charges released from their trap sites [10]. In 2015, Zhao *et al.* found that delayed TEL emission was attributed to the recombination of stored charges accumulated in the devices [11]. Recently, Shikler *et al.* studied the dependence of TEL decay lifetime on the bulk transit time of the charges in polyfluorene-blend-based OLEDs during switch *off* [12].

In this study, we find that the host-molecule transport polarity also plays a key role in charge-carrier dynamic processes and TEL decay behaviors in doped devices. As

is well reported in the literature, the unipolar organic materials transport only one type of carrier dominating the electrical conduction [13], whereas the bipolar materials can simultaneously transport electrons and holes due to the integration of both electron- and hole-transporting moieties in one single molecule [14]. Herein, we observed that the TEL curves measured from devices with bipolar host decay slowly, while the emission tails from devices with unipolar host decay rapidly within a short time range of several microseconds. A series of controlled experiments indicate that the polarity of the host molecule in the doped devices heavily affects the number of accumulated charges in the exciton recombination region (RZ). These accumulated charges can recombine with each other under Coulomb interaction to produce a TEL decay tail after turning off the voltage pulse. Thus, the transport polarity of the host molecule can impact the TEL decay behaviors. Accordingly, this finding supplements an additional factor that can influence the physical microscopic processes of charge carriers and the TEL decay behaviors.

What is more, based on the physical understanding of the influence of the host-molecule polarity on carrier dynamic processes, we find that the devices with different polarities of host exhibit various impacts of emission layer (EML) thickness on the optical-electrical performance. In detail, for devices with a bipolar host, a thicker EML is beneficial for enhancing their optoelectronic performance, consistent with the conclusion of the literature [4]. For devices with a unipolar host, we find that the efficiency roll-off can be significantly suppressed by reducing the EML thickness appropriately. Specifically, the critical current density of J_0 obtains a significant increase from 37.14 to 149.76 mA/cm^2 in the unipolar host-based device by decreasing the EML thickness from 60 to 20 nm. Hence, this study offers another strategy for mitigating the efficiency roll-off of OLEDs, thereby providing valuable insights for improvements in their overall performance.

II. EXPERIMENTAL SECTION

All the control devices under investigation are fabricated on the cleaned glass substrates covered by the anode stripes of indium tin oxide (ITO). The device structures were carried out as ITO/poly(3,4-ethylenedioxythiophene):poly(styrenesulfonate) (PEDOT: PSS, 40 nm)/4,40,40-tris(N-3-methylphenyl-N-phenylamino)triphenylamine (*m*-MTDATA, 60 nm)/host: 5% tetra(t-butyl)rubrene (TBRb) (40 nm)/4,7-diphenyl-1,10-phenanthroline (Bphen, 60 nm)/LiF (1 nm)/Al (100 nm). Herein, the host materials are 4, 4′-N, N′ dicarbazolebiphenyl (CBP), tris (8-hydroxyquinoine) aluminum (Alq$_3$), *m*-MTDATA, and Bphen, respectively. Their molecular structures are shown in Fig. S1 within the Supplemental Material [38]. In addition, Table S1 within the Supplemental Material [38] presents the charge-mobility

values for the four host materials [15–18], and Table S2 within the Supplemental Material [38] lists the device structures. The devices were fabricated in an ultrahigh vacuum chamber (10^{-5} Pa) by organic molecular deposition technique. Among the function layer of these devices, the PEDOT:PSS layer was spin coated on the ITO anode, followed by annealing at 120 °C for 13 min. The other functional layers were subsequently evaporated onto the glass/ITO/PEDOT:PSS substrates by molecular-beam deposition technology. During the deposition processes, a film-thickness monitor (XTM/2) was employed to monitor the deposition rate and thickness of each layer in real time. Following sample preparation, the transient electroluminescence test system, comprising a signal generator (Keithley 4200), a photomultiplier tube, and an oscilloscope (Tektronix DPO7104C), was used to measure the TEL decay data. The pulse width and period were set to 200 μs and 1 ms, respectively. For the measurement of magnetoconductance (MC), the devices were fixed on the cold finger of a closed-cycle cryostat (Janis CCS-350S) that is located between the poles of an electromagnet powered by the Lakeshore EM647 unit with the varied magnetic field from −300 to 300 mT. The bias current flowing through the devices is read by a Keithley 2400 Source Meter.

III. RESULTS AND DISCUSSION

A. Effects of host-molecule polar properties on the TEL attenuation

To study the effects of the host-material polar properties on the device-emission decay behaviors, the TEL decay tails measured from control devs. 1–4, under bias currents from 0.16 to 1.66 mA/cm^2, are shown in Fig. 1. The voltage pulse width and period are fixed at 200 μs and 1 ms, respectively. In addition, the complete TEL waveforms from the voltage pulse *on* to *off* are supplemented in Fig. S2 within the Supplemental Material [38]. Obviously, the TEL curves of these doped devices with various host materials display clear differences in their emission decay tails after turning off the voltage pulse. Specifically, as observed in both Figs. 1(a)–1(d) and S2 within the Supplemental Material [38], the TEL curves of devs. 1–2 decay slowly, whereas the emission tails of devs. 3–4 decay rapidly within a short time range of several microseconds. For a clearer presentation, a comparative analysis of the TEL decay measured from devs. 1–4 operated at bias currents of 0.16 and 1.66 mA/cm^2 are presented in Figs. 1(e) and 1(f). Here, the host materials of devs. 1–2 are CBP and Alq$_3$, respectively [19,20]. Both of them possess bipolar charge-transport properties, with the ability to simultaneously facilitate electron and hole hopping through their respective molecular orbitals. In contrast, the host materials of *m*-MTDATA and Bphen in devs. 3–4 belong to unipolar charge-transport materials,

where the *m*-MTDATA demonstrates a high hole mobility and extremely low electron mobility, while Bphen exhibits the opposite charge-transport ability [17,18]. The charge mobilities of these four distinct organic semiconductor materials have been listed in Table S1 within the Supplemental Material [38]. Based on the observed experimental phenomena, we believe that the host-material transport properties play a key role in the carrier dynamic processes and the formation mechanism of TEL decay. Thus, further investigation will be carried out in the following.

Firstly, the complete TEL waveform curves of devs. 1–4 in Fig. S2 within the Supplemental Material [38] clearly reveal that the delayed emission consists primarily of two components, i.e., a fast emission decay immediately after turning off the voltage pulse and a successive slow emission decay. Therefore, the TEL decay curves can be fitted by using biexponential decay formula with short and long lifetimes, τ_1 and τ_2, respectively.

$$I(t) = A_1 * \exp\left(-\frac{t}{\tau_1}\right) + A_2 * \exp\left(-\frac{t}{\tau_2}\right),$$

where the $I(t)$ refers to the light intensity after turning off the voltage pulse, t means the delay time, and A_1 and A_2 are constants, which represent the proportion of the two components of delayed emission, respectively. Note that, the delay emission mainly originates from the radiative recombination of accumulated charges stored in the emission layer after the voltage pulse is turned off. Therefore, we use exponential functions to fit the decay curves, as also employed in the already reported work [12]. The detailed discussion has been supplemented in Text S1 within the Supplemental Material [38].

The fitting curves and parameters for devs. 1–4 at the current of 0.16 mA/cm^2 are shown in Fig. S3 and Table S3 within the Supplemental Material [38], respectively. Obviously, the TEL lifetime of τ_2 is much longer than τ_1 and the relative proportion of A_2 is higher than that of A_1, especially in devs. 1–2. According to the previous reports, the lifetime of delayed emission generated from TTA is in the order of a few microseconds [3,21]. However, the delayed emission resulting from the radiative recombination of accumulated charges is
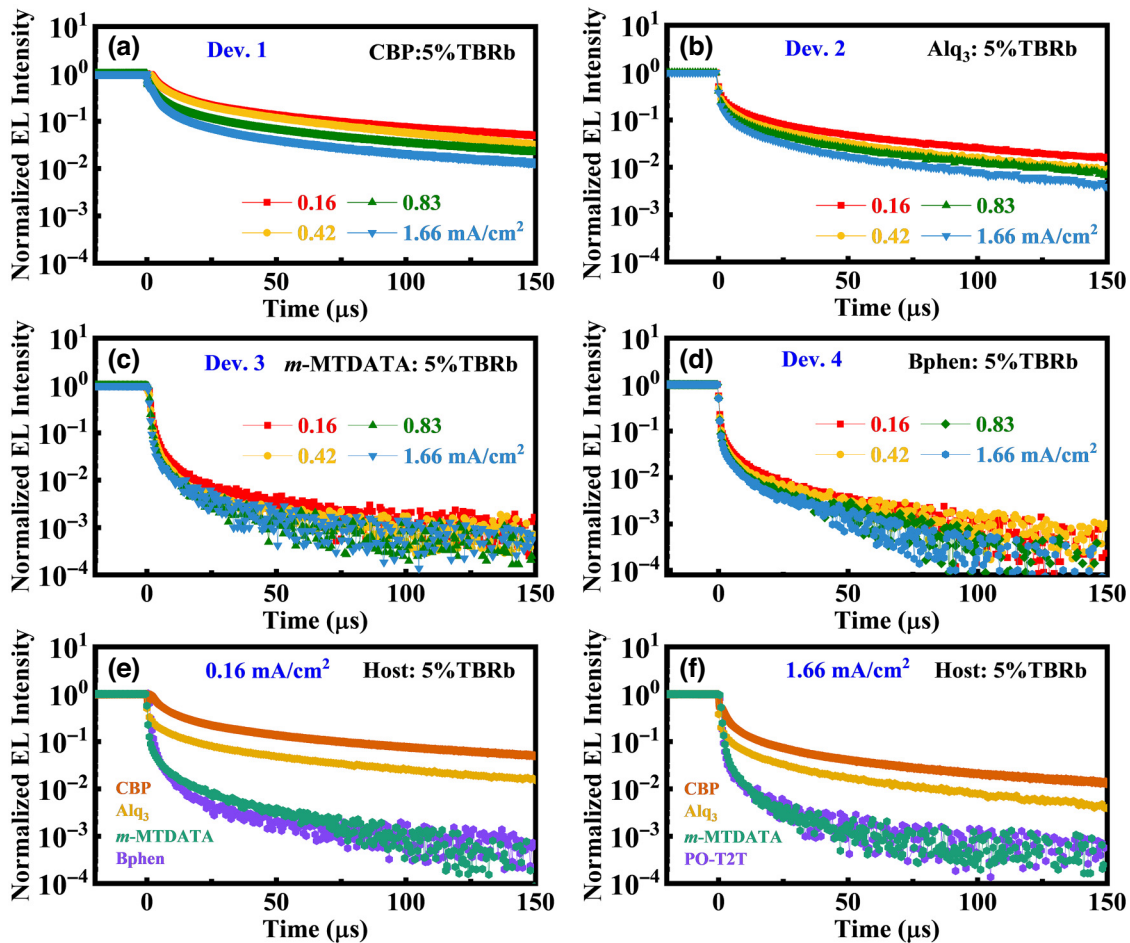

FIG. 1.   (a)–(c) TEL decay characteristics following a 200-μs voltage pulse obtained at the current range from 0.16 to 1.66 mA/cm^2 of dev. 1–4 based on various host materials of CBP, Alq$_3$, *m*-MTDATA, and Bphen, respectively. (e),(f) Comparative analysis of the TEL decay obtained from the four control devices operated at the bias currents of 0.16 and 1.66 mA/cm^2, respectively.
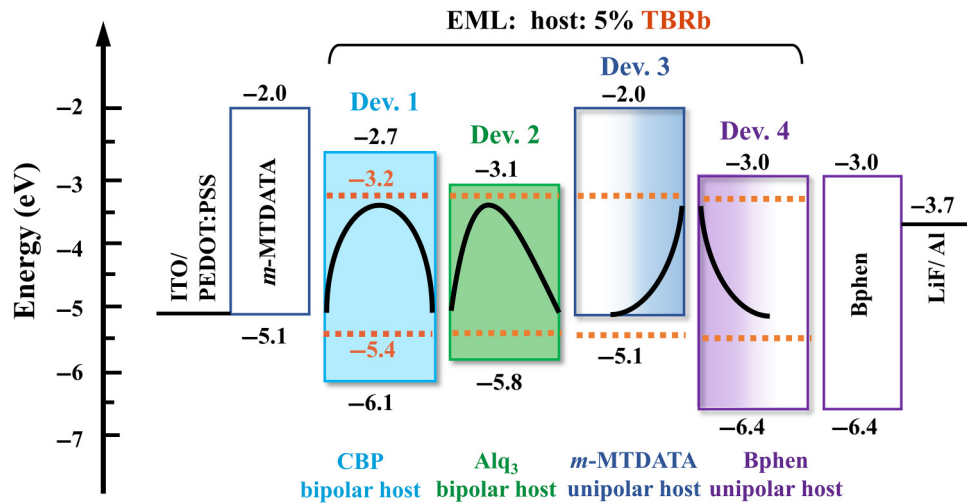
FIG. 2. Schematic diagrams of the energy-level alignments of devs. 1–4 and their exciton recombination zone represented by color fill area in each device. Black lines indicate the expected emission profiles for each device with different host materials.

expected to live longer, which depends on the number of accumulated charges [22,23]. Therefore, we believe that the value of τ_1 relies on the lifetime of excitons, while τ_2 depends on the quantity of the accumulated charges remaining in the EML of OLEDs after turning off the voltage pulse. Herein, we primarily focus on τ_2 due to its higher proportion in the lifetime of the whole TEL delay emission.

In devs. 1–2, the host materials of CBP and Alq$_3$ possess bipolar charge-transport ability, enabling both electrons and holes to be evenly distributed throughout the EML, resulting in a broad RZ, as shown in Fig. 2 (devs. 1–2). After the voltage pulse is turned off, a large number of accumulated charges remain in RZ. The remained charges will generate correlated charge pairs under their Coulomb interaction and then undergo radiative recombination to produce a long-lived TEL delay emission [12,22,24], i.e., a long lifetime of τ_2. However, for devs. 3–4, the values of both τ_1 and τ_2 are very small, especially τ_2 of these two devices are much smaller than those of devs. 1–2. This is because the unbalanced carrier population in the EML of these two devices leads to a narrow RZ and a short exciton lifetime. In dev. 3, the unipolar host material of *m*-MTDATA possesses a greater ability to transport holes than electrons, resulting in an excess of holes and a shortage of electrons in the EML. Consequently, the excitons generated in the narrow RZ nearby EML and electron transport layer (ETL) might be quenched by the excessive holes [25,26], leading to a small value of τ_1. On the other hand, after pulse off, the remaining accumulated charges in dev. 3 include a large number of holes but very few electrons, resulting in a small number of residual electron-hole pairs available for radiative recombination, which in turn causes a remarkable decrease in the value of τ_2. Similarly, the excitons in dev. 4 might be quenched by excessive

electrons, and the narrow RZ moves toward the hole transport layer (HTL) and EML side. Additionally, we have detected the position of RZ in devs. 1–4 from the measured EL spectra. The detailed discussions have been supplemented in Text S2 within the Supplemental Material [38]. In summary, the bipolar transport host in EML facilitates the charge balance, resulting in a wide RZ. A substantial number of accumulated charges are stored in the wide RZ. Conversely, devices with a unipolar transport host result in a narrow RZ, accompanied by fewer accumulated charges within this confined region.

To directly detect the charge accumulation in OLEDs with different polar hosts, the capacitance-voltage (*C-V*) curves for the control devs. 1–4 are measured and presented in Fig. S4 within the Supplemental Material [38]. The geometric capacitance (C_0) from these four devices are almost equal to each other due to their same device thicknesses [27]. In conjunction with the further experimental findings and pertinent literature reports [2,27], we believe that the first peak in *C-V* curve is generated by the accumulated charges stored at the interfaces between the charge-transport layer (CTL) and EML due to the existence of the energy barrier, while the second peak is produced by the accumulated charges trapped on the dopant molecules within EML. The detailed discussion of the generation mechanisms of the peaks in *C-V* curves has been supplemented in Text S3 within the Supplemental Material [38]. Obviously, from Fig. S4 within the Supplemental Material [38] we can see that the amplitude of second peaks of devs. 1–2 is clearly greater than those of devs. 3–4, indicating that devs. 1–2 with a bipolar host possess more accumulated charges in their EML than those of devs. 3–4 with a unipolar host. Consequently, these accumulated charges in devs. 1–2 with the broad RZ will undergo radiative recombination after the voltage pulse is
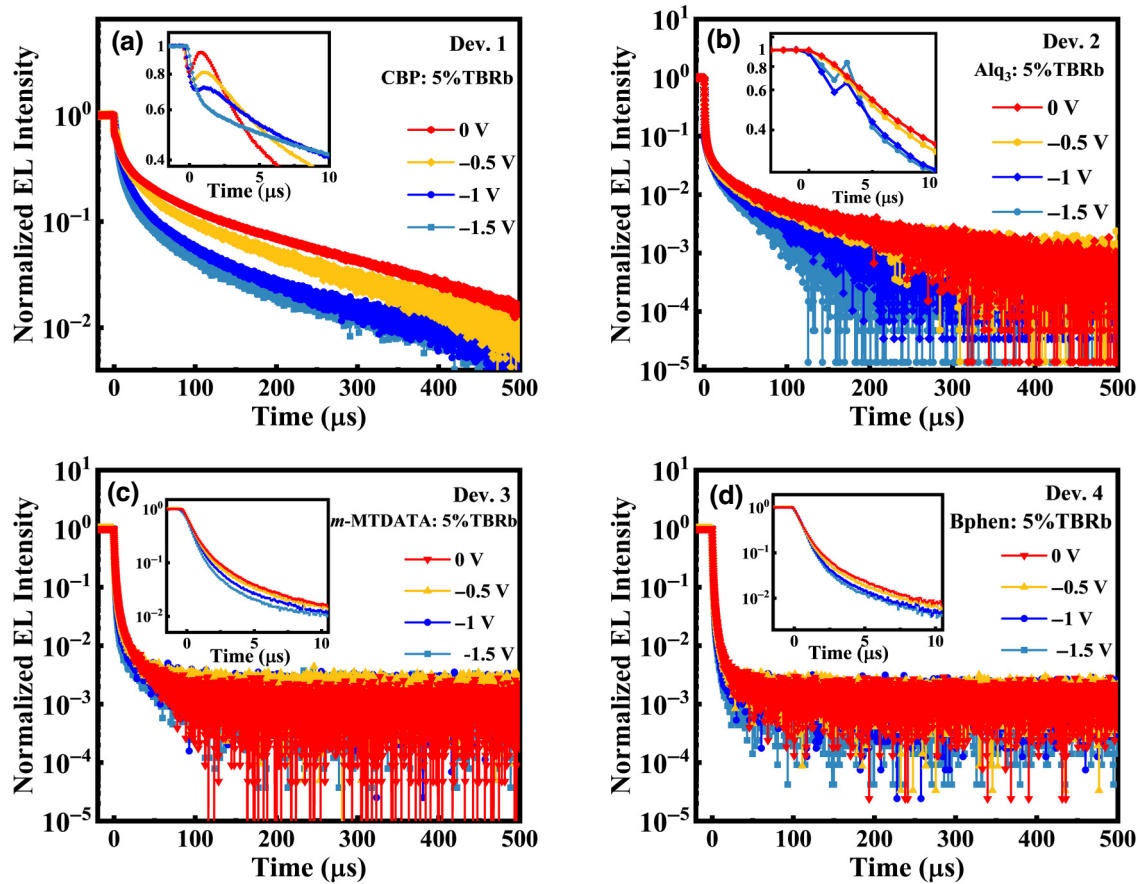
FIG. 3. TEL signals of devs. 1–4 after the voltage pulse is turned off and different reverse voltages are applied in the *off* state (from 0 to −1.5 V). Insert: detailed information at the TEL falling edge. The applied voltage pulse waveforms have been depicted in Fig. S5 within the Supplemental Material [38].

turned off, producing long-lived delayed luminescence, as shown in Figs. 1(a) and 1(b).

Moreover, comparing the TEL decay behaviors in Figs. 1(a)–1(d), the current dependences of these curves from devs. 1–4 are different from each other. Specifically, the TEL curves of devs. 1–2 present a faster decay with the increasing current, while these of devs. 3–4 are insensitive to the change of current. This is because devs. 1–2 have wide RZ, a part of electrons and holes pass through RZ without recombination and then accumulate near the opposite interface when a larger electric field is applied. The separation of electrons and holes in a wide RZ reduces their recombination probability after pulse off, resulting in a faster TEL decay in the case of larger bias currents. However, considering that the host of *m*-MTDATA and Bphen in devs. 3–4 belong to unipolar charge-transfer materials, the electrons and holes in their narrow RZ cannot be separated far from each other, even under a large electric field. Therefore, the TEL delayed emission from devs. 3–4 does not change obviously with the varied currents.

To again demonstrate the influence of the host-molecule transport properties on the charge distribution and RZ position, we conducted the applied-reverse-voltage-modulated TEL decay profiles of devs. 1–4. On the whole, the applied voltage changing from 0 to −1.5 V promotes the TEL decay of devs. 1–2, while it has a negligible impact on that of devs. 3–4. Specifically, as shown in Figs. 3(a) and 3(b), a clear faster attenuation is observed with an increasing reverse voltage. Furthermore, as depicted in the inserts of Figs. 3(a) and 3(b), the peak appears and enhances with an increasing reverse voltage applied to the device after turning off the positive pulse voltage. Here, both the faster decay and enhanced peak are attributed to the accelerated recombination of the accumulated charges remaining in RZ under the applied reverse electric field. This phenomenon is consistent with most conclusions reported in the literature [28,29]. However, for devs. 3–4 with narrow RZ shown in Fig. 3, only a small amount of accumulated charge remains in their RZ after the pulse voltage is turned off. Consequently, the application of negative pulse voltage has virtually no impact on their emission decay.
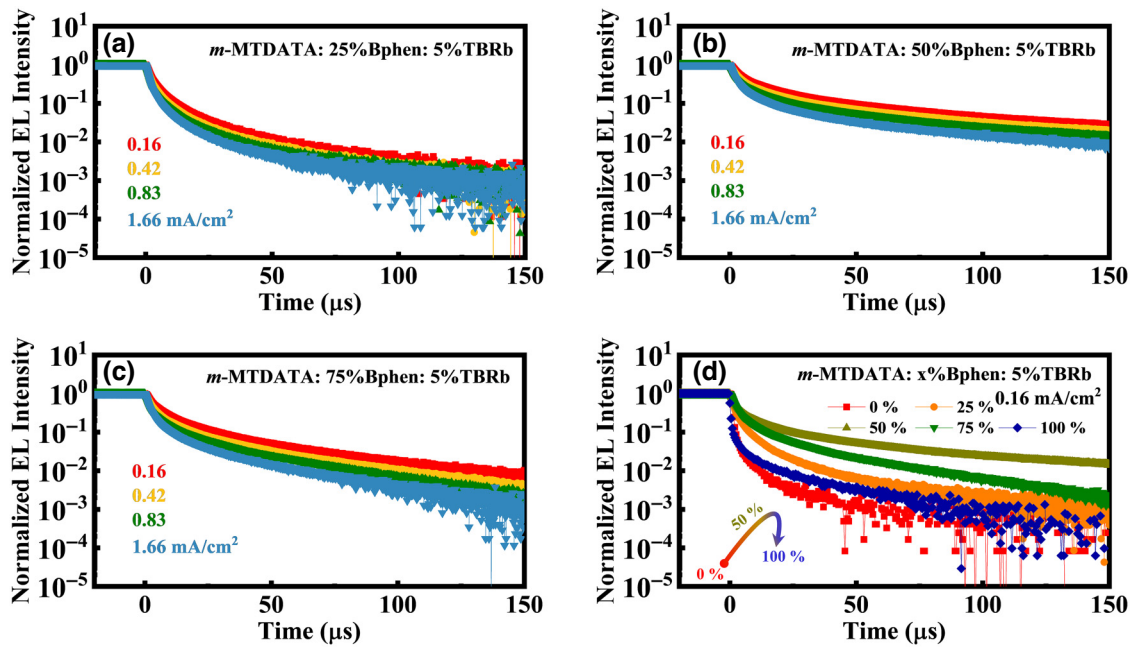
FIG. 4. (a)–(c) The current dependence of TEL decay acquired from the devices with different unipolar electron-hole transport materials mixing ratios in the EML operated at the current range of 0.16–1.66 mA/cm². (d) The EL decay profiles of these devices at 0.16 mA/cm² with varied mixture ratios from 0% to 100%. Here the mixture ratios of 0% and 100% correspond to the case of dev. 3 and dev. 4 in Figs. 1(c) and 1(d), respectively.

To date, the expected exciton RZ in the devices with different host materials has been established in the schematic diagram of Fig. 2. When the host of the device possesses bipolar charge-transport properties, the positive and negative charges in the EML are approximately balanced, resulting in a wide RZ that can almost uniformly occupy the entire EML (devs. 1–2 in Fig. 2). However, when a unipolar charge-transport material serves as the host, the unbalanced charges in the EML lead to a narrow RZ (devs. 3–4 in Fig. 2). In addition, we find that the TEL decay behavior and its current dependence can characterize the charge-balance degree and RZ width of OLEDs as discussed in part of Figs. 1 and 3. A wide RZ including the enormous population of accumulated charges will produce a longer TEL decay lifetime and present a clearer current dependence on TEL decay. Therefore, through observing the TEL decay behaviors and their current dependence, we will further investigate the influence of the transport properties of host materials on charge balance in the EML.

Based on the aforementioned analysis, an excess of holes and a deficiency of electrons exist in the EML of dev. 3 due to the inherent hole-transporting characteristics of the host material of *m*-MTDATA. To achieve charge balance, it is desirable to mix a proper proportion of an electron transport material (Bphen) into the EML of dev. 3. The mixing ratios of *m*-MTDATA: x% Bphen are set to 25%, 50%, and 75%. Firstly, as shown in Figs. 1(c), 4(a)–4(c), and 1(d), as the blending ratios increase from 0% to 100%, the current dependence of the TEL decay

curves changes from being insensitive to current to a faster decay with increasing current, and finally back to being insensitive to current. These results indicate that with the increasing blending ratio, the EML of these devices undergoes the transitions from a hole-rich state to the charge balance and then to an electron-rich state. In other words, the RZ of these devices initially widens and then narrows, which is consistent with our expectations. In addition, the TEL decay trend of these devices with different blending ratios of *m*-MTDATA: x% Bphen provides more powerful proof for the variation of RZ. From Fig. 4(d), we can observe that as the blending ratio increases, the TEL tails initially enhance followed by a subsequent reduction. The strongest delayed emission occurs when the blending ratio is 1:1 ($x = 50$%). This experiment result again demonstrates the imbalance of charges in EML when a unipolar material acts as a host of the doped OLEDs (devs. 3 and 4). However, as reported in the literature, the unbalanced charges are harmful to the device's performance [26]. Taking dev. 3 in Fig. 2 as an example, the excessive holes in the EML would dissociate excitons through triplet-charge annihilation (TQA) process, resulting in a reduction in external quantum efficiency (EQE) and an exacerbation of efficiency roll-off. Fortunately, we find that reducing the EML thickness of dev. 3 can efficiently boost its charge balance to improve the device performance. It is worth noting that different host-transport devices exhibit various impacts of EML thickness on their optical-electrical performance. Further investigations about the

influence of EML thickness on the charge balance and photoelectric performance will be conducted in the following sections.

B. Influences of the EML thickness on the charge balance in devices with different host-transport properties

Figures 5(a) and 5(b) present the influence of the EML thickness on TEL decay behaviors of dev. 1 and dev. 3, respectively. For dev. 1, the emission decay of the 20-nm-thick EML device becomes faster compared with those of 40-nm- and 60-nm-thick EML devices. However, TEL decay of dev. 3 shows inconspicuous changes with the decrease in the EML thickness. The reason for this phenomenon is that the RZ of dev. 3 is inherently narrow even in a wide EML due to the extremely weak electron transport capability of the host material (*m*-MTDATA). Thus, reducing the EML thickness almost does not affect the RZ width and the number of remaining electron-hole pairs. Meanwhile, with the decreasing EML thickness, the excessive holes accumulated in the EML but outside the RZ would be gradually eliminated, thus improving charge balance and suppressing the TQA process.

To visualize the TQA process induced by unbalanced charges in these two devices with different EML thicknesses, magnetoconductance (MC) responses of the devices have been measured and depicted in Figs. 5(c) and 5(d). As can be seen, MC traces are composed of low-field effects (LFEs, $|B| \leq 9$ mT) and high-field effects (HFEs, $9 < |B| \leq 300$ mT). The LFEs characterize the evolution processes between singlet and triplet excitons, including intersystem crossing (ISC) and reverse ISC (RISC), which are, respectively, distinguished by inverted and upright Lorentzian line shapes within several millitesla around zero magnetic field (B) [30]. The HFEs represent the TQA process. It is widely documented that the gradual increase and decrease of the HFEs, characterized by a FWHM approximately in the range of 100 mT, can be ascribed to the B-suppressed scattering and dissociation channels of the TQA process, respectively [31–34]. On the one hand, the scattering channel pertains to the scattering of excessive electrons by triplet states ($e + T_1 \rightarrow e + S_0$). Obviously, the scattering channel can reduce the current intensity flowing through the device by reducing electron mobility. The applied B will suppress this scattering channel to conversely enhance the current. Consequently, the HFEs exhibit an increasing trend with the increased magnetic field. On the other hand, the dissociation channel is associated with the dissociation of triplet states induced by excessive holes ($h + T_1 \rightarrow h + e + h$). Accordingly, the dissociation channel can augment the current through increasing the population of free electrons and holes. The B-suppressed dissociation channel weakens the device bias current, resulting in a reduction in HFEs [35]. On the whole, the TQA process can generate in both electron-excessive and hole-excessive devices. Their differences are
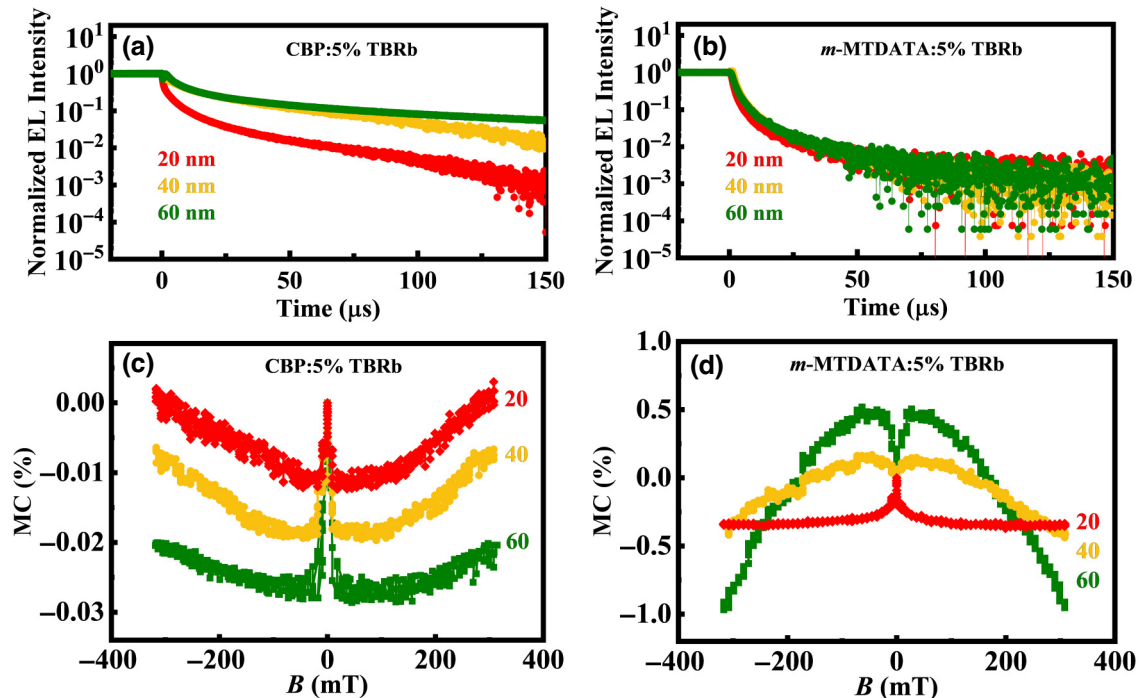

FIG. 5. (a),(b) TEL decay curves from dev. 1 and dev. 3 with the EML thicknesses from 20 to 60 nm. (c),(d) MC(B) responses from these two control devices with the EML thicknesses from 20 to 60 nm. The operational current of all devices is fixed at 0.16 mA/cm^2.
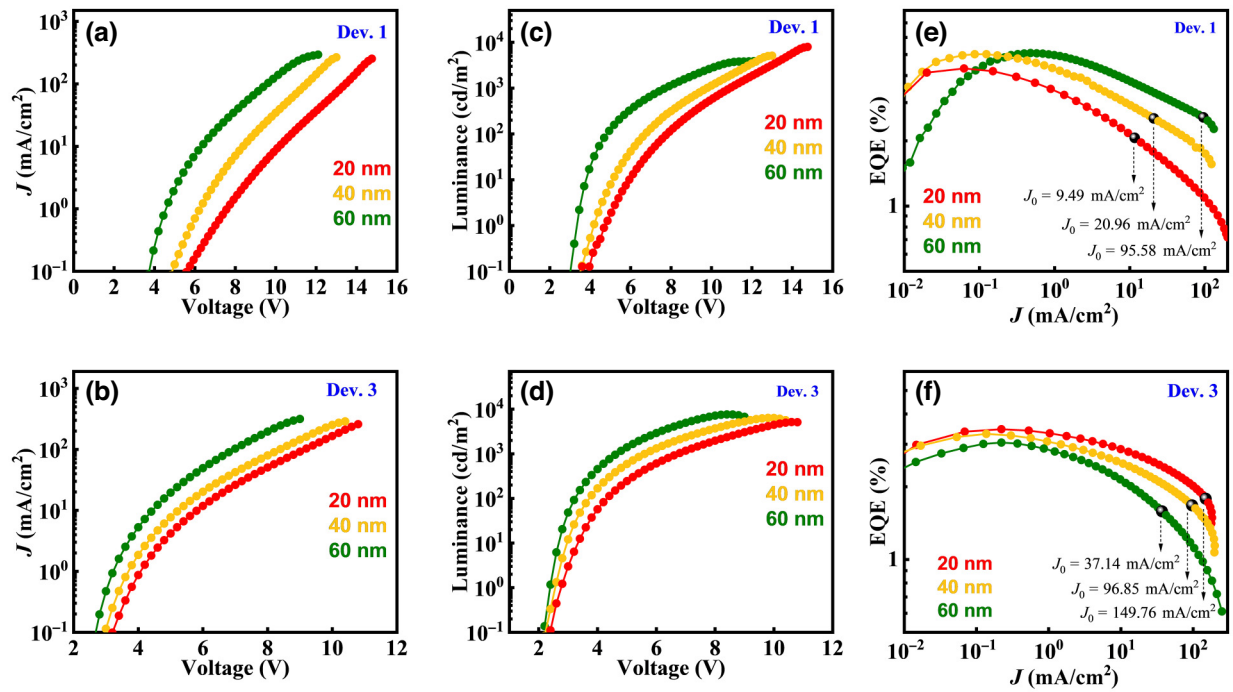
FIG. 6. (a)–(d) Current density-voltage (J-V) and luminance-voltage (L-V) curves of dev. 1 and dev. 3 with the EML thickness decreasing from 60 to 20 nm. (e),(f) External quantum efficiency-current density (EQE-J) curves of these devices. J_0 represents the current density at which the EQE drops to half of its maximum value.

mainly revealed by an increasing or decreasing magnitude of the MC curves with the enhancement of the magnetic field, respectively. In Fig. 5(c), the MC responses of dev. 1 exhibit RISC and TQA fingerprint curves induced by excessive electrons. Firstly, in the devices with a thinner EML, the RISC evolution process from triplet to singlet weakens, while the TQA process enhances. The enhanced TQA is attributed to the increase in charge density and exciton density within a thinner EML when the devices are driven by the same applied current. Furthermore, the consumption of triplet excitons by TQA process inhibits RISC process. This is consistent with the experiment conclusion drawn from Fig. 5(a). For dev. 3, with the decreasing EML thickness from 60 to 20 nm, the reduction of TQA and the transition from ISC to RISC confirms that the excessive holes are remarkably eliminated in the devices with a thinner EML. In other words, with the decreasing thickness of the EML, the degree of charge balance in dev. 3 is improved. This implies that when using unipolar charge-transport materials as the host of doped OLEDs, it is advisable to reduce the EML thickness appropriately in order to achieve the charge balance. In general, balanced charges existing in the EML is beneficial for the improvement of the device performance. In fact, the photoelectric performance of dev. 3 indeed has been improved by appropriately reducing the EML thickness. The detailed electroluminescence characteristics of dev. 1 and dev. 3 have been studied in below.

C. Electroluminescence characteristics of the doped devices with bipolar and unipolar transport hosts

The current density-voltage (J-V), luminance-voltage (L-V), and external quantum efficiency-current density (EQE-J) characteristics of dev. 1 with different EML thicknesses are shown in Figs. 6(a), 6(c), and 6(e), respectively. The corresponding performance of dev. 3 is displayed in Figs. 6(b), 6(d), and 6(f). The relevant photoelectric parameters and efficiency roll-off information of these devices are listed in Tables S4 and S5 within the Supplemental Material [38]. In the tables, the term "turn-on voltage" means the voltage value at the luminance of 1 cd/m^2, while "critical current density, J_0" refers to the current density at which the EQE drops to 50% of its maximum value [7]. Similar to the most reported variation trend in the literature [36,37], the turn-on voltage of both dev. 1 and dev. 3 is decreased with a thinner EML. However, the maximum current efficiency of dev. 1 with a bipolar host (CBP) exhibits a decrease as the EML thickness is reduced from 60 to 20 nm. More terribly, the reduction in the EML thickness seriously exacerbates the efficiency roll-off from the J_0 of 95.58 to 9.49 mA/m^2. The reason for the deteriorated efficiency roll-off can be well explained by the enhanced TQA as shown in Fig. 5(c). In the contrast, the photoelectric performances of dev. 3 with a unipolar transport host (*m*-MTDATA) in Figs. 6(c) and 6(d) show a positive improvement with the decreasing EML thickness. The EQE has been slightly enhanced. Of note, the

efficiency roll-off is significantly suppressed. J_0 obtains a significant increase from 37.14 to 149.76 mA/cm^2 by decreasing the EML thickness from 60 to 20 nm. This is attributed to the elimination of excessive charges in the EML, as discussed in Figs. 2 and 5(d). In addition, the maximum luminescence (L_{max}) has also been obviously improved with the decreasing EML thickness. Overall, based on the above analysis of the optoelectronic performance of doped OLEDs with bipolar and unipolar transport hosts, the following conclusions can be drawn. For devices with a bipolar host, a thicker EML is beneficial for enhancing their optoelectronic performance. However, for devices with a unipolar host, reducing the EML thickness appropriately can significantly improve the device performance.

IV. CONCLUSION

In summary, we proposed that the TEL measurement tool can serve as an effective experimental method to elucidate the complex charge-carrier dynamic processes in the doped OLEDs possessing different host-molecule transport polarities. Additionally, we found that the TEL decay behavior of these doped devices is closely related to the charge-balance degree in their EML. In devices with bipolar transport host materials, their TEL decay emission exhibits a long-lived delay fluorescence with a lifetime of around 50 μs. This is because the relatively balanced charge distribution within the EML results in a long exciton lifetime and a wide exciton RZ. After switching down the voltage pulse, the long-lived triplet excitons generate delay fluorescence through TTA process. Moreover, a great amount of residual charges in the RZ undergo radiative recombination by Coulomb interactions. Thus, the collective contribution of these two delay emission components produces the long-lived TEL decay from the devices with bipolar transport host materials. In addition, in this kind of device, their TEL decay presents a clear current dependence that the TEL emission decays faster under a bigger operational current. Contrarily, for devices with unipolar transport hosts, their TEL emissions decay rapidly within the time range of 10 μs. In these devices, the charge-carrier population in the EML is extremely unbalanced. On one hand, triplet excitons are susceptible to quenching by free charge carriers, leading to a diminishment of TTA. On the other hand, the number of residual electron-hole pairs available for radiative recombination in the narrow RZ is quite small after turning off the voltage pulse. Accordingly, the TEL curves from the devices with unipolar transport hosts exhibit a fast decay after turning off the voltage pulse. Note that, the delay fluorescence from TTA is not the main component of the TEL delay emission, instead, the radiative recombination of accumulated charges plays a dominant role in the delay emission. On the whole, all of these TEL decay behaviors in different doped OLEDs are affected by the transport properties of the host molecules. Based on the full understanding of the impact of the host-molecule transport properties on carrier dynamic processes, we successfully suppress the efficiency roll-off by adjusting the device structure to improve the charge balance degree. Specifically, it is advisable to increase the EML thickness appropriately in devices with bipolar host materials, while devices with unipolar host materials should undergo suitable thinning of the EML. Therefore, this work not only deepens the physical understanding of the effect of host-molecule polar properties on the TEL decay and efficiency roll-off of doped OLEDs, but also provides another idea for designing high-performance organic optoelectronic devices.

[1] C. W. Tang and S. A. VanSlyke, Organic electroluminescent diodes, Appl. Phys. Lett. **51,** 913 (1987).

[2] J.-H. Lee, S. Lee, S.-J. Yoo, K.-H. Kim, and J.-J. Kim, Langevin and trap-assisted recombination in phosphorescent organic light emitting diodes, Adv. Funct. Mater. **24,** 4681 (2014).

[3] R. Ieuji, K. Goushi, and C. Adachi, Triplet–triplet upconversion enhanced by spin–orbit coupling in organic light-emitting diodes, Nat. Commun. **10,** 5283 (2019).

[4] C. Murawski, K. Leo, and M. C. Gather, Efficiency roll-off in organic light-emitting diodes, Adv. Mater. **25,** 6801 (2013).

[5] D. Di, L. Yang, J. M. Richter, L. Meraldi, R. M. Altamimi, A. Y. Alyamani, D. Credgington, K. P. Musselman, J. L. MacManus-Driscoll, and R. H. Friend, Efficient triplet exciton fusion in molecularly doped polymer light-emitting diodes, Adv. Mater. **29,** 1605987 (2017).

[6] Y. Zhang and S. R. Forrest, Triplets contribute to both an increase and loss in fluorescent yield in organic light emitting diodes, Phys. Rev. Lett. **108,** 267404 (2012).

[7] M. A. Baldo, C. Adachi, and S. R. Forrest, Transient analysis of organic electrophosphorescence. II. Transient analysis of triplet-triplet annihilation, Phys. Rev. B **62,** 10967 (2000).

[8] J. Chen, X. Zhao, X. Tang, Y. Ning, F. Wu, X. Chen, H. Zhu, and Z. Xiong, An unprecedented spike of the electroluminescence turn-on transience from guest-doped OLEDs with strong electron-donating abilities of host carbazole groups, Mater. Horiz. **8,** 2785 (2021).

[9] D. Y. Kondakov, Characterization of triplet-triplet annihilation in organic light-emitting diodes based on anthracene derivatives, J. Appl. Phys. **102,** 114504 (2007).

[10] Z. Gan, R. Liu, R. Shinar, and J. Shinar, Transient electroluminescence dynamics in small molecular organic light-emitting diodes, Appl. Phys. Lett. **97,** 113301 (2010).

[11] C. Zhang, S. Zhao, Z. Xu, X. Hong, Z. Long, P. Wang, Y. Chen, and X. Xu, The storage of charges and its optical application in organic light-emitting diodes measured by a transient electroluminescence method, Org. Electron. **27**, 114 (2015).

[12] N.-B. Shiran, G. Dor, Y. Adi, and S. Rafi, Relating transient electroluminescence lifetime and bulk transit time in OLED during switch-off, J. Mater. Chem. C **6**, 972 (2020).

[13] H. H. Fong and S. K. So, Hole transporting properties of tris(8-hydroxyquinoline) aluminum (Alq$_3$), J. Appl. Phys. **100**, 094502 (2006).

[14] X. Qiao, Y. Tao, Q. Wang, D. Ma, C. Yang, L. Wang, J. Qin, and F. Wang, Controlling charge balance and exciton recombination by bipolar host in single-layer organic light-emitting diodes, J. Appl. Phys. **108**, 034508 (2010).

[15] H. Li, L. Chen, J. Qiao, L. Duan, D. Zhang, G. Dong, L. Wang, and Y. Qiu, Experimental and theoretical study of the charge transport property of 4,4′-N,N′-dicarbazole-biphenyl, Sci. China Chem. **55**, 2428 (2012).

[16] A. Fuchs, T. Steinbrecher, M. S. Mommer, Y. Nagata, M. Elstner, and C. Lennartz, Molecular origin of differences in hole and electron mobility in amorphous Alq3—a multi-scale simulation study, Phys. Chem. Chem. Phys. **14**, 4259 (2012).

[17] A. Bucinskas, O. Bezvikonnyi, R. Durgaryan, D. Volyniuk, A. Tomkeviciene, and J. V. Grazulevicius, New m - MTDATA skeleton-based hole transporting materials for multi-resonant TADF OLEDs, Phys. Chem. Chem. Phys. **24**, 27847 (2022).

[18] S. Naka, H. Okada, H. Onnagawa, and T. Tsutsui, High electron mobility in bathophenanthroline, Appl. Phys. Lett. **76**, 197 (2000).

[19] S. Naka, H. Okada, H. Onnagawa, Y. Yamaguchi, and T. Tsutsui, Carrier transport properties of organic materials for EL device operation, Synth. Met. **111–112**, 331 (2000).

[20] T. Yamada, F. Suzuki, A. Goto, T. Sato, K. Tanaka, and H. Kaji, Revealing bipolar charge-transport property of 4,4′-N,N′-dicarbazolylbiphenyl (CBP) by quantum chemical calculations, Org. Electron. **12**, 169 (2011).

[21] N. C. Erickson and R. J. Holmes, Engineering efficiency roll-off in organic light-emitting devices, Adv. Funct. Mater. **24**, 6074 (2014).

[22] Q. Huang, S. Zhao, Z. Xu, X. Fan, C. Shen, and Q. Yang, Exciplex emission and decay of co-deposited 4,4′,4″-tris[3-methylphenyl(phenyl)amino]triphenylamine:tris-[3-(3-pyridyl)mesityl]borane organic light-emitting devices with different electron transporting layer thicknesses, Appl. Phys. Lett. **104**, 161112 (2014).

[23] C. Zhang, Z. Xu, P. Wang, Z. Qin, S. Wageh, A. Al-Ghamdi, and S. Zhao, A new benchmark of charges storage in single-layer organic light-emitting diodes based on electrical and optical characteristics, Molecules **26**, 741 (2021).

[24] J. Li, B. Qiao, S. Zhao, D. Song, C. Zhang, and Z. Xu, Investigation on OLEDs efficiency roll-off with interfacial charge storage and their time-resolved emission spectra, Org. Electron. **83**, 105756 (2020).

[25] H. van Eersel, P. A. Bobbert, R. A. J. Janssen, and R. Coehoorn, Effect of Forster-Mediated triplet-polaron quenching and triplet-triplet annihilation on the efficiency roll-off of organic light-emitting diodes, J. Appl. Phys. **119**, 163102 (2016).

[26] X. Zhao, X. Tang, H. Zhu, C. Ma, Y. Wang, S. Ye, L. Tu, and Z. Xiong, Room-temperature observation for reverse intersystem crossing in exciplex-based OLEDs with balanced charge injection, ACS Appl. Electron. Mater. **3**, 3034 (2021).

[27] V. Shrotriya and Y. Yang, Capacitance–voltage characterization of polymer light-emitting diodes, J. Appl. Phys. **97**, 054504 (2005).

[28] S. Lee, K.-H. Kim, D. Limbach, Y.-S. Park, and J.-J. Kim, Low roll-off and high efficiency orange organic light emitting diodes with controlled co-doping of green and red phosphorescent dopants in an exciplex forming co-host, Adv. Funct. Mater. **23**, 4105 (2013).

[29] N. R. Al Amin, K. K. Kesavan, S. Biring, C.-C. Lee, T.-H. Yeh, T.-Y. Ko, S.-W. Liu, and K.-T. Wong, A comparative study via photophysical and electrical characterizations on interfacial and bulk exciplex-forming systems for efficient organic light-emitting diodes, ACS Appl. Electron. Mater. **2**, 1011 (2020).

[30] F. Wu, X. Zhao, H. Zhu, X. Tang, Y. Ning, J. Chen, X. Chen, and Z. Xiong, Identifying the exciplex-to-exciplex energy transfer in tricomponent exciplex-based OLEDs through magnetic field effect measurements, ACS Photonics **9**, 2713 (2022).

[31] X. Zhao, J. Chen, X. Tang, F. Wu, Y. Ning, X. Chen, and Z. Xiong, Conversions from normal to abnormal current-dependent ISC and from abnormal to normal current-dependent RISC processes in exciplex-based OLEDs, Adv. Mater. Interfaces **9**, 2200155 (2022).

[32] B. Hu and Y. Wu, Tuning magnetoresistance between positive and negative values in organic semiconductors, Nat. Mater. **6**, 985 (2007).

[33] X. Tang, R. Pan, X. Zhao, W. Jia, Y. Wang, C. Ma, L. Tu, and Z. Xiong, Full confinement of high-lying triplet states to achieve high-level reverse intersystem crossing in rubrene: A strategy for obtaining the record-high EQE of 16.1% with low efficiency roll-off, Adv. Funct. Mater. **30**, 2005765 (2020).

[34] D. Ma, Utilization of hot excitons to fabricate high efficiency blue fluorescence organic light-emitting diodes, Org. Electron. **121**, 106854 (2023).

[35] K.-W. Tsai, T.-H. Lee, J.-H. Wu, J.-Y. Jhou, W.-S. Huang, S.-N. Hsieh, T.-C. Wen, T.-F. Guo, and J. C. A. Huang, Antagonistic responses between magnetoconductance and magnetoelectroluminescence in polymer light-emitting diodes, Org. Electron. **14**, 1376 (2013).

[36] M. R. Fadavieslam, The effect of thickness of light emitting layer on physical properties of OLED devices, Optik **182**, 452 (2019).

[37] J. Ni, T. Tano, Y. Ichino, T. Hanada, T. Kamata, N. Takada, and K. Yase, Organic light-emitting diode with TiOPc layer–a new multifunctional optoelectronic device, Jpn. J. Appl. Phys. **40**, L948 (2001).

[38] See Supplemental Material at http://link.aps.org/supplemental/10.1103/PhysRevApplied.20.054034 for additional data descriptions of the complete TEL curves, capacitance, MEL responses from devs. 1-4 and the reasons for employing exponential functions to fit the TEL decay curves.